PNAS RESEARCH ARTICLE | PHYSIOLOGY OPEN ACCESS

KCNQ1 is an essential mediator of the sex-dependent perception of moderate cold temperatures

Aytug K. Kiper[a], Sven Wegner[a], Aklesso Kadala[b], Susanne Rinné[a], Sven Schütte[a], Zoltán Winter[b], Mirjam A. R. Bertoune[c], Filip Touska[b], Veronika Matschke[d], Eva Wrobel[e], Anne-Kathrin Streit[a], Florian Lang[f], Constanze Schmidt[g], Eric Schulze-Bahr[h], Martin K.-H. Schäfer[c], Jakob Voelkl[i], Guiscard Seebohm[d,h], Katharina Zimmermann[b,1], and Niels Decher[a,1,2]

Affiliations are included on p. 9.

Edited by Joseph Takahashi, The University of Texas Southwestern Medical Center, Dallas, TX; received December 20, 2023; accepted April 25, 2024

Low temperatures and cooling agents like menthol induce cold sensation by activating the peripheral cold receptors TRPM8 and TRPA1, cation channels belonging to the TRP channel family, while the reduction of potassium currents provides an additional and/or synergistic mechanism of cold sensation. Despite extensive studies over the past decades to identify the molecular receptors that mediate thermosensation, cold sensation is still not fully understood and many cold-sensitive peripheral neurons do not express the well-established cold sensor TRPM8. We found that the voltage-gated potassium channel KCNQ1 (Kv7.1), which is defective in cardiac LQT1 syndrome, is, in addition to its known function in the heart, a highly relevant and sex-specific sensor of moderately cold temperatures. We found that KCNQ1 is expressed in skin and dorsal root ganglion neurons, is sensitive to menthol and cooling agents, and is highly sensitive to moderately cold temperatures, in a temperature range at which TRPM8 is not thermosensitive. C-fiber recordings from *KCNQ1*$^{-/-}$ mice displayed altered action potential firing properties. Strikingly, only male *KCNQ1*$^{-/-}$ mice showed substantial deficits in cold avoidance at moderately cold temperatures, with a strength of the phenotype similar to that observed in *TRPM8*$^{-/-}$ animals. While sex-dependent differences in thermal sensitivity have been well documented in humans and mice, *KCNQ1* is the first gene reported to play a role in sex-specific temperature sensation. Moreover, we propose that KCNQ1, together with TRPM8, is a key instrumentalist that orchestrates the range and intensity of cold sensation.

menthol | *KCNQ1* knockout mice | cold sensation | C-fibers | temperature behavior assay

The odorant alcohol menthol has been used for decades as a chemical analog to induce cold sensation when studying peripheral cold detection and perception (1). Accordingly, menthol was also used as a tool compound during the discovery of the first cold-sensitive receptor, namely the *Transient Receptor Potential Melastatin Subtype 8* (TRPM8) channel (2). In the meantime, TRPM8 was recognized as a key sensory receptor for menthol-induced cold sensitization in somatosensory afferents. However, many cold-sensitive peripheral neurons of the mouse do not express TRPM8 (3) and three independent studies identified residual menthol and cold sensitivity in *TRPM8* deficient mice (4–6). The subsequent studies have attributed some of this function to the irritant and noxious cold receptor TRPA1 (7, 8). Indeed, TRPM8 and TRPA1 act synergistically in the detection of cold (TRPM8) and painful cold (TRPA1), as evidenced by the cold avoidance deficits observed in mice lacking both TRPM8 and TRPA1 (9). Although another TRP channel, namely TRPC5, has been initially described as a putative sensor for moderate cold temperatures (10), over the years, it has become evident that this channel primarily acts in the signaling of cold-pain in teeth (11).

While TRP channels contribute to the depolarizing calcium inward currents in cutaneous nociceptors and thermoreceptors, some members of the two-pore domain potassium (K_{2P}) channel family (TREK-1, TREK-2, TRAAK, and TRESK) were discussed to modulate peripheral cold sensing by regulating temperature-dependent excitability in general (12–14) or in the case of TASK-3, by directly modulating TRPM8-dependent cold sensing (15). Similarly, inhibition of voltage-gated K^+ channels contributes to depolarization by limiting cationic outward currents and can potently enhance TRPM8-dependent cold responses (16) and tune their activation threshold (17). However, the isolated knock-out of *TREK-1* or *TRAAK* does not affect cold sensitivity and the respective mice show no obvious phenotype concerning temperature sensation (12, 18). In addition, *TREK-2*$^{-/-}$ and *TRESK*$^{-/-}$ knock-out mice have only a somewhat enhanced sensitivity to moderately cold temperatures (13, 14).

Despite extensive research in the field of temperature sensation and TRP channels, there is still a lack of a primary temperature sensor in the moderate cold temperature

Significance

Despite extensive studies over the past decades to identify the mechanism of temperature sensation, there is still a lack of understanding of the molecular sensors involved in cold sensation. We found that the voltage-gated potassium channel KCNQ1 (Kv7.1), which forms together with KCNE1 the cardiac delayed rectifier potassium current I_{Ks}, is in addition to its known function in the heart, a highly relevant and sex-specific sensor of moderately cold temperatures. Based on the newly identified functional expression in C-fibers, the substantial temperature- and menthol-sensitivity, together with the strong in vivo effects on cold avoidance, we propose a novel extracardiac function for KCNQ1 channels, namely the perception of moderate/ambient cold temperatures in a sex-dependent manner.

Author contributions: A.K.K., K.Z., and N.D. designed research; A.K.K., S.W., A.K., S.R., S.S., Z.W., M.A.R.B., F.T., V.M., E.W., A.-K.S., C.S., E.S.-B., M.K.-H.S., and G.S. performed research; F.L. and J.V. contributed new reagents/analytic tools; A.K.K., S.W., A.K., S.R., S.S., Z.W., M.A.R.B., F.T., A.-K.S., and K.Z. analyzed data; and A.K.K., S.W., K.Z., and N.D. wrote the paper.

The authors declare no competing interest.

This article is a PNAS Direct Submission.

[1]K.Z. and N.D. contributed equally to this work.

[2]To whom correspondence may be addressed. Email: decher@staff.uni-marburg.de.

This article contains supporting information online at https://www.pnas.org/lookup/suppl/doi:10.1073/pnas.2322475121/-/DCSupplemental.

Published June 10, 2024.

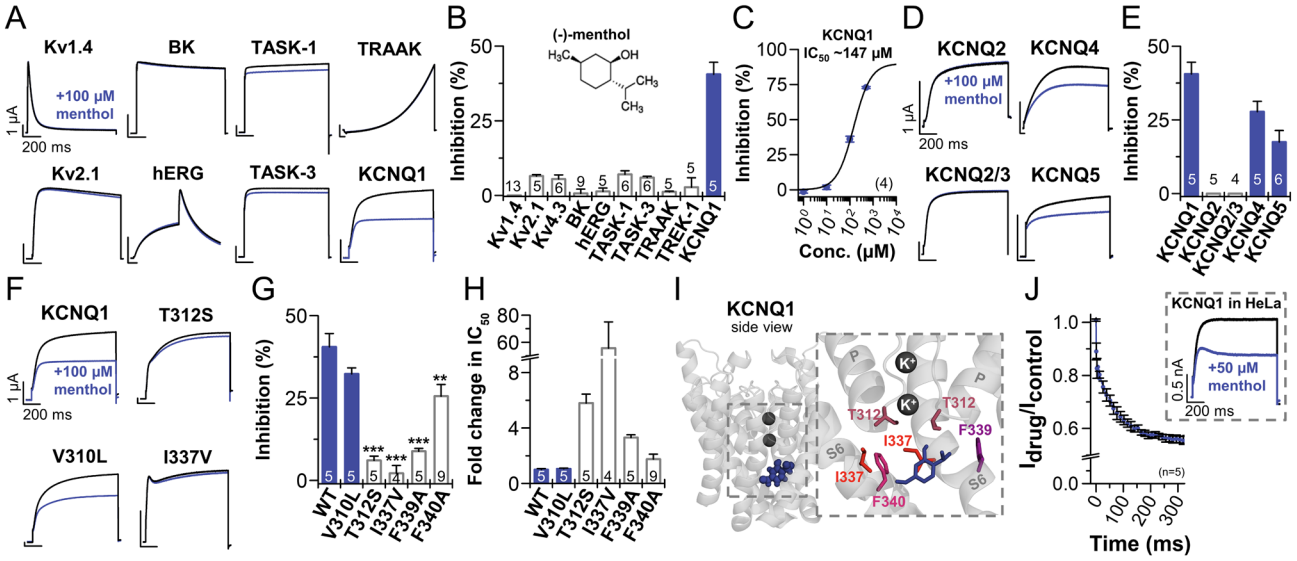

Fig. 1. Menthol is an open channel blocker of KCNQ1 channels. (*A*) Representative current traces of two-electrode voltage-clamp recordings from an array of potassium channels before (black) and after (blue) application of 100 µM (-)-menthol. (*B*) Analysis of the channel inhibition by application of 100 µM (-)-menthol. (*C*) A dose–response curve of menthol on KCNQ1 currents, calculated using a fit to the Hill equation. (*D*) Representative current traces of other KCNQ channel family members before and after (-)-menthol application, similar to *A*. (*E*) Analysis of the channel inhibition by application of 100 µM (-)-menthol. (*F*) Representative current traces of wild-type KCNQ1 and mutants of the lower selectivity filter (T312S, V310L) or central cavity (I337V). (*G*) Analysis of the channel inhibition by application of 100 µM (-)-menthol. (*H*) Fold change in IC_{50} compared to wild-type KCNQ1. (*I*) Illustration of an energy-optimized docking solution of menthol in the central pore of a KCNQ1 homology model. An enlargement of the region indicated as dashed box is depicted as inset. Hydrogen bondings are expected with T312 and I337, while hydrophobic interactions are predicted at residues T312, I337, F339, and F340. (*J*) The onset of channel block was analyzed in HeLa cells and calculated by dividing the current traces after drug treatment by the current traces under control conditions ($I_{drug}/I_{control}$). The *inset* illustrates representative current traces of whole-cell patch-clamp recordings from HeLa cells transfected with cDNA encoding the human KCNQ1 channel, before (black) and after (blue) application of 50 µM menthol. The number of biological replicates (n) is indicated within the graphs. Data are presented as mean ± SEM. $^{**}P < 0.01$, $^{***}P < 0.001$ by Student's *t* test.

range. Also, K_{2P} channels, as introduced above, do not functionally cover this temperature range in a satisfactory manner, since only weak changes in temperature sensitivity of the animals were observed after deletion of the respective genes. In addition, K_{2P} channels are not polymodal or menthol-sensitive. Thus, given the ability of mammals to polymodally sense temperature and menthol in the moderate cold temperature range, there should be another yet unknown highly relevant temperature sensor active in this temperature range. Since TRP channels were already exhaustively studied, we started our search for a polymodal temperature sensor with an in vitro screen for a menthol-sensitive potassium channel. Note that sex-dependent differences in thermal sensitivity have been well documented in humans and mice (19–21), but also here little is known about the genes involved in sex-specific temperature sensation, therefore we carefully studied both sexes individually.

Strikingly, we revealed the voltage-gated and estrogen/testosteron-regulated KCNQ1 potassium channel (also denoted as Kv7.1 or KvLQT1) (22–25) as menthol- and temperature-sensitive in the moderate cold temperature range. Note that KCNQ1 is primarily known as part of the slowly activating potassium current complex (I_{Ks}) (26, 27) that was previously associated with the cardiac LQT1 syndrome (28). Moreover, we describe in the present study a major and sex-dependent contribution of KCNQ1 to the in vivo perception of moderate cold temperatures.

Results

Identification of KCNQ1 as a Menthol-Sensitive Potassium Channel. Since mammals can polymodally sense temperature and menthol in the moderate cold temperature range, we first screened an extensive array of potassium channels in *Xenopus laevis* oocytes for their sensitivity to (-)-menthol (Fig. 1 *A* and *B*). In voltage-clamp recordings, we observed little or no inhibition of the voltage-dependent potassium (Kv) channels Kv1.4, Kv2.1, and Kv4.3 or the K_{2P} channels TASK-1, TASK-3, TREK-1, TRAAK-1, the calcium-dependent BK channel, or hERG (Kv11.1). However, a prominent current reduction was observed for the KCNQ1 channel with an IC_{50} of 147.2 ± 11.8 µM (Fig. 1*C*), which, to our surprise, was in the same concentration range as for TRPM8 channels. Note that the EC_{50} of menthol for TRPM8 when studied in oocytes was 196 ± 22 µM (29). Interestingly, the KCNQ1 channel was also sensitive to the cold ligand icilin and the menthol analog WS-12, especially WS-12 inhibited the KCNQ1 channel with an IC_{50} of 3.5 µM (*SI Appendix*, Fig. S1). The KCNQ family consists of five family members, namely, KCNQ1-5. Similar to KCNQ1, KCNQ4 and KCNQ5 currents were blocked by 100 µM (-)-menthol (Fig. 1 *D* and *E*). In contrast, KCNQ2/KCNQ3 heterodimeric channels that contribute to the neuronal "M-current" (30) were not sensitive in this concentration range in the *Xenopus* oocyte expression system (Fig. 1 *D* and *E*). To gain a better understanding of the mechanism of KCNQ1 inhibition by (-)-menthol, we examined mutants in the channel pore that are part of the previously described open channel blocker binding site in KCNQ1, including V310L and T312S of the lower selectivity filter and I337V, F339A, and F340A of the S6 segment (31). Recordings of the mutants T312S, I337V, F339A, and F340A, showed significantly reduced (-)-menthol sensitivity compared to wild-type (Fig. 1 *F–H*), with T312S and I337V exhibiting the most potent change in IC_{50}. Interestingly, the isoleucine residue at position 337 is not conserved in KCNQ2 and KCNQ3 channels (*SI Appendix*, Fig. S2). Instead, these channels have a valine residue at this position, which may contribute to the reduced (-)-menthol sensitivity of both channels. Taken together, these data suggest that (-)-menthol binds to the central cavity and most likely acts as a classical open channel blocker.

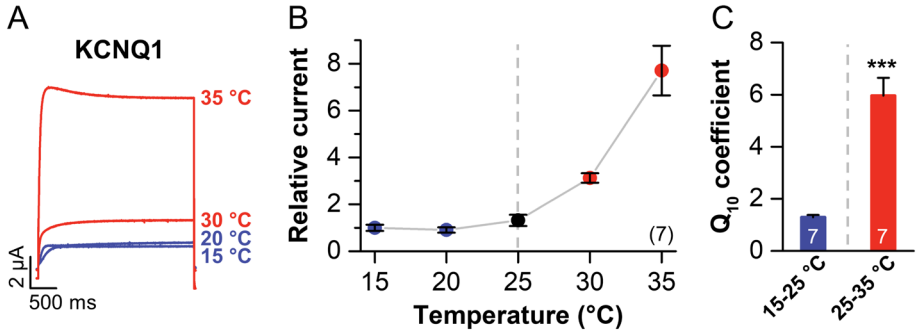

Fig. 2. Temperature sensitivity of KCNQ1 channels. (*A*) To investigate the temperature sensitivity of KCNQ1 channels, the bath temperature was successively increased during two-electrode voltage-clamp recordings of KCNQ1 in *Xenopus* oocytes. Illustration of representative current traces of KCNQ1 recorded at four different temperatures. (*B*) A plot of the relative current versus the temperature obtained in KCNQ1 recordings analyzing the peak currents at the end of a 3 s test pulse. The dashed line indicates the separation of the two temperature ranges (15 to 25 °C and 25 to 35 °C) for which the Q_{10} values were calculated. (*C*) Q_{10} values obtained in the temperature range from 15 to 25 °C (blue) and 25 to 35 °C (red). The number of biological replicates (n) is indicated within the graphs. Data are presented as mean ± SEM. *$P < 0.05$ by Student's *t* test.

This hypothesis was further supported by molecular docking experiments using a KCNQ1 homology model (Fig. 1*I*). The best docking solution, with an energy-minimized position of the drug, suggests that menthol binds in the central cavity below the selectivity filter. Here, menthol is likely to form hydrogen bonds with T312 of the pore signature sequence, while the compound is stabilized by hydrophobic interactions, e.g., with I337 of the S6 segment. Furthermore, we investigated the blocking kinetics of menthol in transiently transfected HeLa cells. Here, we utilized a classical method to analyze blocking kinetics, in which the currents after drug application were divided by the currents under control conditions ($I_{drug}/I_{control}$), in order to mathematically eliminate the channel activation that overlaps with the channel block (32). Utilizing this analysis, we noted that the channels have to fully open (ratio 1.0) before the menthol block can develop over time, as typically seen for open channel blockers (Fig. 1*J*). Thus, we propose that (-)-menthol acts as an open channel blocker of the KCNQ1 channel with residues I337, T312, and F339 as an essential part of the binding site.

KCNQ1 Is Temperature Sensitive in the Moderately Cold Temperature Range. The temperature sensitivity of I_{Ks}, encoded by the KCNQ1 channel together with its ß-subunit KCNE1 (26, 27), was already described in previous studies (33–35), whereas the temperature-sensitivity of KCNQ1 alone was only sparsely studied (35). Thus, we next tested whether the current amplitudes of KCNQ1 expressed alone are also sensitive to cold temperatures. In voltage-clamp recordings of oocytes expressing KCNQ1, we applied a continuous voltage-step protocol from −80 mV to +40 mV while increasing the bath temperature from 15 to 35 °C (Fig. 2 *A* and *B*). We calculated the temperature coefficient Q_{10} to quantify the temperature sensitivity. This analysis revealed that KCNQ1 is not particularly temperature sensitive at cold temperatures (15 to 25 °C), whereas the channels are highly sensitive at moderately cold temperatures (25 to 35 °C) (Fig. 2*C*) with a Q_{10} of approximately 6. In contrast, TRPM8 is not temperature sensitive in this range, displaying a Q_{10} of only about 3 (36), which is a value close to that for most non-thermosensitive biological processes (37). Conversely, TRPM8 is highly sensitive to cold temperatures (15 to 25 °C) (36). Taken together, these data suggest that KCNQ1 may have the propensity to sense temperature changes efficiently in the moderate/ambient cold temperature range, at which TRPM8 channels do not efficiently sense temperature changes.

Expression of KCNQ1 Channels in Skin and Dorsal Root Ganglion Neurons. While the expression and function of KCNQ2–KCNQ5 channels in the peripheral nervous system have been extensively studied, neuronal KCNQ1 channels were so far only associated with epilepsies (38) and the sensorineural deafness associated with the recessive LQT1 syndrome (Jervell–Lange Nielsen) (39). To explore the potential of KCNQ1 to contribute to temperature sensation in the peripheral nervous system, we analyzed its expression in skin and dorsal root ganglion (DRG) neurons. RT-PCR experiments revealed that KCNQ1 is expressed in human skin (Fig. 3 *A* and *B*), which is consistent with its previously reported protein expression in the human protein atlas (40). Ion channels generally have a much lower mRNA expression than the established "housekeeping" genes. Therefore, we compared the expression of KCNQ1 with that of TRPM8. The semiquantitative pixel-densitometry analysis of four independent RT-PCRs revealed that the mRNA expression of KCNQ1 is highly similar to that of TRPM8 (Fig. 3*B*). Next, we analyzed the expression in sensory neurons and probed for a putative coexpression of KCNQ1 in subpopulations of TRPM8-expressing C-fibers. To this end, we revalidated the specificity of the most commonly used KCNQ1 antibody using transfected HeLa cells and dissociated DRG cultures from *KCNQ1*$^{-/-}$ mice (*SI Appendix,* Fig. S3). Consistent with mRNA and protein expression in skin, we clearly detected KCNQ1 proteins in the soma of DRG neurons (Fig. 3*C*), whereas the specific fluorescent signals were lost in *KCNQ1*$^{-/-}$ mice (*SI Appendix,* Fig. S3 *B* and *C*), leaving only weak autofluorescence (*SI Appendix,* Fig. S3 *B* and *C*). In addition, we analyzed KCNQ1 by immunohistochemistry in dissociated DRG cultures of *TRPM8*$^{EGFPf/EGFPf}$ mice (Fig. 3 *C–E*). Here, we identified TRPM8 in 6% of the DRG neurons, with an average surface area of approximately 805 µm^2, while another population of neurons was positive for KCNQ1. The subpopulation of KCNQ1 positive cells was found at the same frequency as TRPM8-positive neurons (6%), with a similar mean area of approximately 717 µm^2 (Fig. 3 *C–E*). Only 1% of the cells were positive for both KCNQ1 and TRPM8 (Fig. 3*D*). Taken together, our experiments reveal a population of KCNQ1-positive DRG neurons that are as abundant as but distinct from TRPM8-positive DRG neurons. These data are consistent with previous findings that many cold-sensitive peripheral neurons of the mouse do not express TRPM8 (3), as mentioned above. Our observations were further supported during the progress of our study by data from large-scale single-cell RNA sequencing

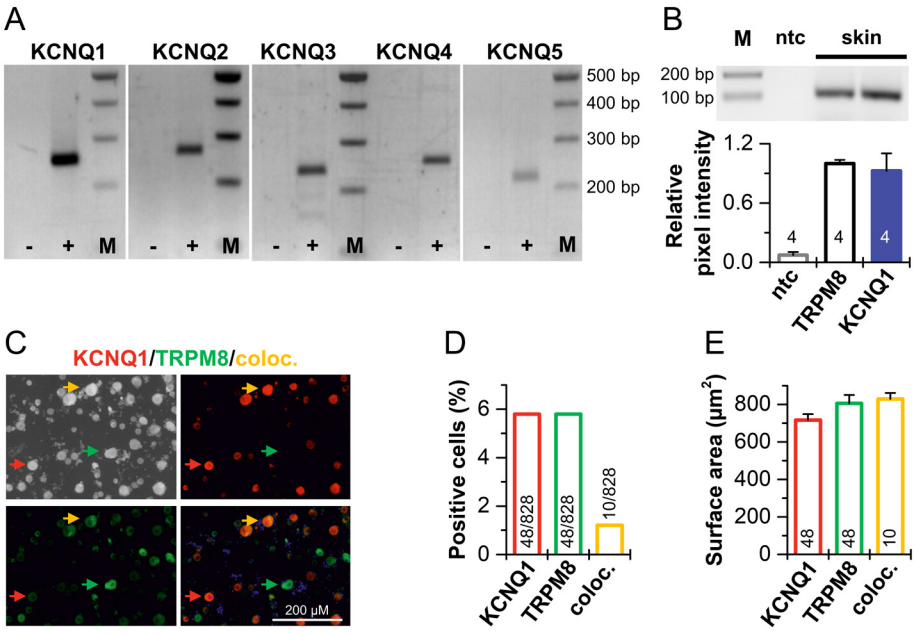

Fig. 3. Expression of KCNQ1 channels in skin and DRG neurons. (*A*) KCNQ1-5 mRNA expression in human skin analyzed using RT-PCR experiments. Primers were designed to amplify ~220 to 260 bp fragments. M: Marker; -: no template control. (*B*) Semiquantitative RT-PCR of KCNQ1 and TRPM8 from human skin (*Upper* panel). Primers were designed to amplify ~110 bp fragments. The *Lower* panel illustrates the respective pixel-densitometry analysis from four independent RT-PCRs, normalized to the pixel intensity of TRPM8. M: Marker; ntc: no template control. (*C*) Quantification of TRPM8 and KCNQ1 coexpression in cultured DRG neurons from a *TRPM8*$^{EGFPf/EGFPf}$ mouse. Representative confocal images illustrating, from *Top Left* to *Bottom Right*, background image, KCNQ1 positive cells in red (representative cell with red arrow), TRPM8 EGFP cells in green (representative cell with green arrow), and colocalization of both channels (yellow arrows). (*D*) Bar graph of the percentage of positive cells. The number of counted cells is indicated in the bar graphs. (*E*) Bar graph of the size of positive cells. The number of KCNQ1 and/or TRPM8 positive cells is indicated in the bar graphs.

studies in mice, in which the authors found that KCNQ1, but not the regulatory KCNE1 subunit, is predominantly expressed in cold-sensitive C-fiber low-threshold mechanoreceptors (C-LMTR) (41, 42), a neuronal subpopulation that is clearly distinct from those expressing TRPM8. Given that KCNQ1 is expressed in temperature-sensitive somatosensory neurons, the question arises whether the menthol- and temperature-sensitive KCNQ1 channels play a role in physiological cold sensation.

Reduced Cold Avoidance and Altered C-Fiber Cold Response in Male *KCNQ1*$^{-/-}$ Mice. Next, we investigated the role of KCNQ1 channels in physiological cold sensation in vivo by characterizing the temperature preference behavior of *KCNQ1*$^{-/-}$ mice. As in humans and mice, sex-dependent differences in thermal sensitivity were reported (19–21), the two sexes were studied separately. We used a circular temperature gradient assay with an eight-zone configuration of the temperature gradient ring, as this has been previously proven as most adequate to characterize the cold avoidance deficit in TRPM8$^{-/-}$ mice (43). Interestingly, male *KCNQ1*$^{-/-}$ mice displayed a strongly reduced cold avoidance over time, with animals remaining at significantly lower preferred temperatures in the second half of the experiment, while wild-type littermates spent progressively more time in the 21 to 34 °C temperature range (Fig. 4 *A–C*). Thus, overall, male *KCNQ1*$^{-/-}$ mice remained at cooler floor temperatures. To our surprise, this impaired cold avoidance was similarly strong as observed in *TRPM8* knock-out mice (43). Next, we analyzed the temperature preference of female *KCNQ1*$^{-/-}$ mice and their wild-type littermates using the same assay. Strikingly, the female transgenic animals did not yield any signs of altered temperature preference at any point in time (Fig. 4 *D–F*). This apparent difference between the two sexes is also very evident in the plot of the cumulative response function (Fig. 4 *G–J*). Thus, we identified *KCNQ1* as one of the first genes involved in sex-specific temperature sensation.

Finally, we further investigated the phenotype of male *KCNQ1*$^{-/-}$ mice in situ at the primary afferents. Here, we recorded the electrical activity of mechanosensitive C-fibers of the skin isolated from *KCNQ1*$^{-/-}$ mice or wild-type littermates. C-fibers were screened for cold sensitivity and lack of heat response. We used a standardized 60 s cold stimulus to the receptive field to quantify cold responses (9). Overall, we found significantly smaller cold responses in *KCNQ1*$^{-/-}$ mice with lower activation thresholds and reduced mean discharge rates, as illustrated in Fig. 5, because membrane depolarization mediated by the KCNQ1 inhibition is lacking. Similar results were previously observed in *TRPM8*$^{-/-}$ mice (9), as cold receptors from *TRPM8*$^{-/-}$ mice no longer responded to a cold stimulus with an increase in action potential frequency, due to lack of TRPM8-mediated receptor potential. Taken together, KCNQ1-deficient C-fibers display striking encoding deficits.

In conclusion, given the strong temperature sensitivity of KCNQ1 in the range of 25 to 35 °C and the effects in our in vivo assays, KCNQ1 potassium channels might fill a gap to primarily sense moderate/ambient cold temperatures, while TRP channels primarily detect cold (TRPM8) and noxious cold (TRPA1) temperatures (Fig. 6).

Discussion

Here, we demonstrate that the KCNQ1 channel is menthol- and temperature-sensitive, and the altered cold responses of *KCNQ1*$^{-/-}$ mice suggest that this potassium channel is, alongside TRPM8, one of the most relevant cold sensors and the most potent known thermosensor at moderately cold temperatures, while its expression and/or function in the peripheral nervous system has been hardly studied so far. With advances in single-cell RNA sequencing, as mentioned above, expression of KCNQ1 in cold-sensitive C-LTMRs neurons of the mice has been identified during the last steps of our study (41, 42). These results should be taken with

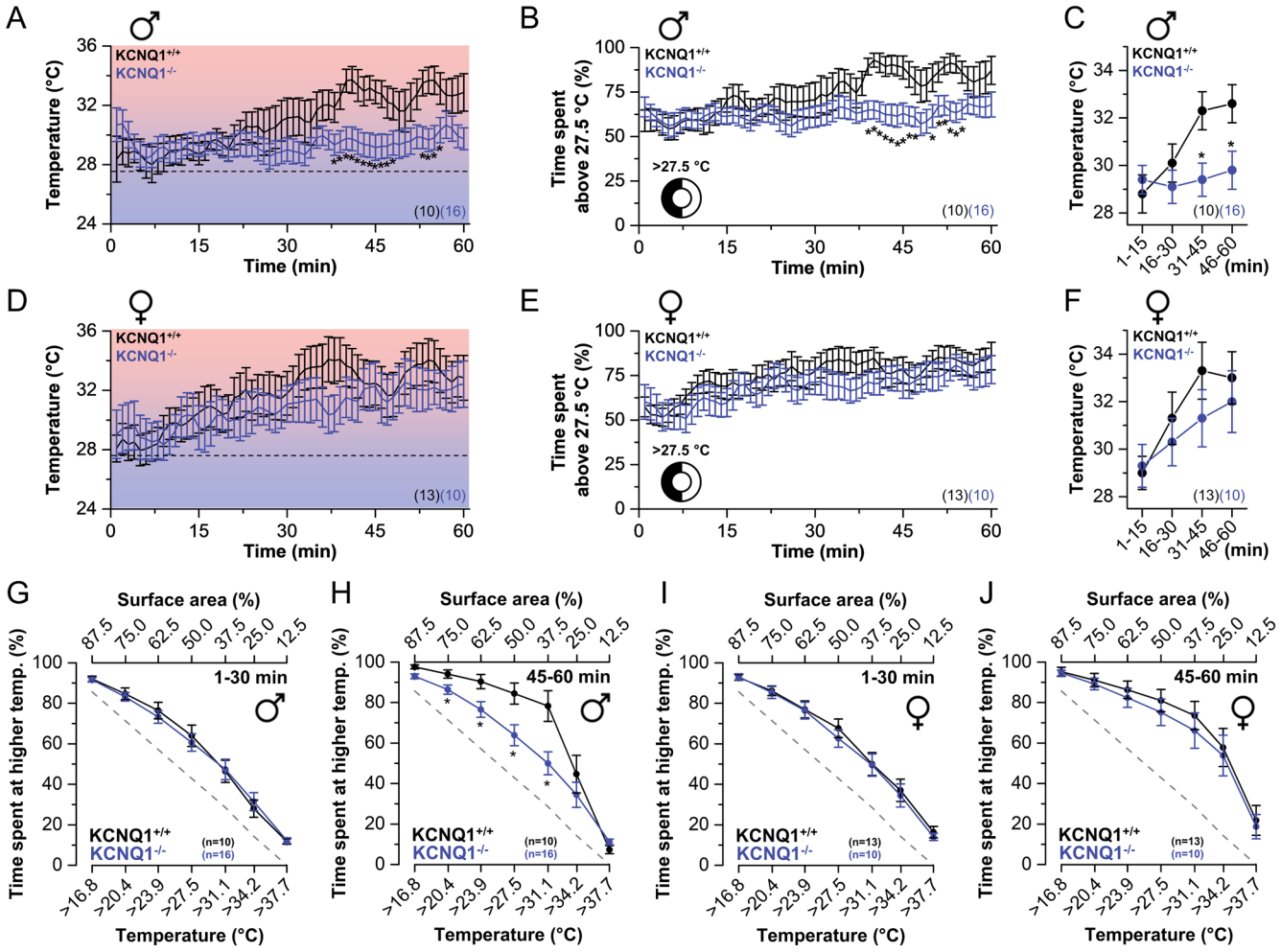

Fig. 4. Reduced cold avoidance in male *KCNQ1*$^{-/-}$ mice. (*A*) The preferred temperature of the mice over a time course of 60 min, illustrated for males. The dashed black line illustrates the average temperature the assay would yield, if mice would not prefer a certain temperature and randomly move in the circular assay. (*B*) The time course of temperature selection of *KCNQ1*$^{-/-}$ and *KCNQ1*$^{+/+}$ illustrates the percentage of time spent in the warmer semicircle, i.e., above 27.5 °C, in males. The sketch illustrates the semicircle and floor surface above 27.5 °C. (*C*) Weighted temperature preference in 15-min bins for males. (*D*) The same as in (*A*), but illustrated for females. (*E*) The same as in (*B*), but illustrated for females. (*F*) The same as in (*C*), but illustrated for females. (*G–J*) Cumulative response functions of time spent (in %) above different temperatures in the thermal ring. The cumulative surface area of the temperature zones above a given temperature is indicated as an upper *X* axis. The lower *X* axis represents the temperature of the eight zones in the ring assay; the *Y* axis indicates the percentage of time each group of animals spent above the indicated temperature zone, the upper *X* axis illustrates the corresponding fraction of the floor surface, and the dashed gray line represents the expected a random nonselection behavior. (*G* and *I*) Comparison of male (*G*) and female (*I*) *KCNQ1*$^{+/+}$ (black) and *KCNQ1*$^{-/-}$ (blue) mice during the first 30 min (data are mostly reflecting the exploratory behavior). (*H* and *J*) Comparison of male (*H*) and female (*J*) *KCNQ1*$^{+/+}$ (black) and *KCNQ1*$^{-/-}$ (blue) mice during the last 15 min (time 45 to 60 after start) (time course at which animals select their preferred temperature). The number of biological replicates (n) is shown in each panel. Data presented as mean ± SEM. *$P < 0.05$ by ANOVA.

caution, as the correlation between mRNA levels and corresponding protein levels has been debated in the literature for many years. However, recent studies have shown that mRNA levels are often maintained at the protein level (44, 45) and the correlation between mRNA levels and corresponding protein levels is exceptionally high for transmembrane proteins such as ion channels (46). In contrast to our results, a previous study, investigating KCNQ protein expression in rat DRG neurons, revealed an expression of KCNQ2-5 but not KCNQ1 (47). These conflicting results toward the expression of KCNQ1 in DRGs might be explained by the fact that KCNQ1 was recently reported to be preferentially expressed in a particular subset of cold-sensitive DRG neurons (C-LTMRs) (41, 42) and/or differences in expression patterns between rat and mice.

Other members of the KCNQ channel family were studied toward their potential role in temperature sensation. Rivas-Ramírez et al. demonstrated that the M-current contributes to the resting membrane potential of sympathetic neurons at physiological (37 °C) but not at room (23 °C) temperatures (48). This ability of KCNQ2/KCNQ3 channels to sense temperature becomes directly evident as inhibition of peripheral M-currents enhances cold transduction in native nociceptors (16). The effects on temperature sensation were primarily/solely attributed to "neuronal" KCNQ2/3 channels, despite the known expression of KCNQ1 in the central nervous system (38). This is critical in general, as the pharmacological tools previously used to study M-currents in cold sensation also modify KCNQ1 channels (49, 50).

Menthol has been extensively utilized as a pharmacological tool to identify TRPM8 channels in native tissue (51–55). However, the menthol sensitivity of KCNQ1 is similar or even higher than that of TRPM8. In addition, KCNQ1 is also expressed in DRG neurons, similar to TRPM8 channels, although in a different cell population (41, 42). Thus, the conclusion to assign the effects of menthol to either TRPM8 or KCNQ1 channels must be drawn with caution, and previously obtained data might, in some cases, require reevaluation. The here-identified menthol sensitivity of KCNQ1 is not only relevant to avoid misinterpretations in the future toward the physiological role of TRPM8, but it can also be

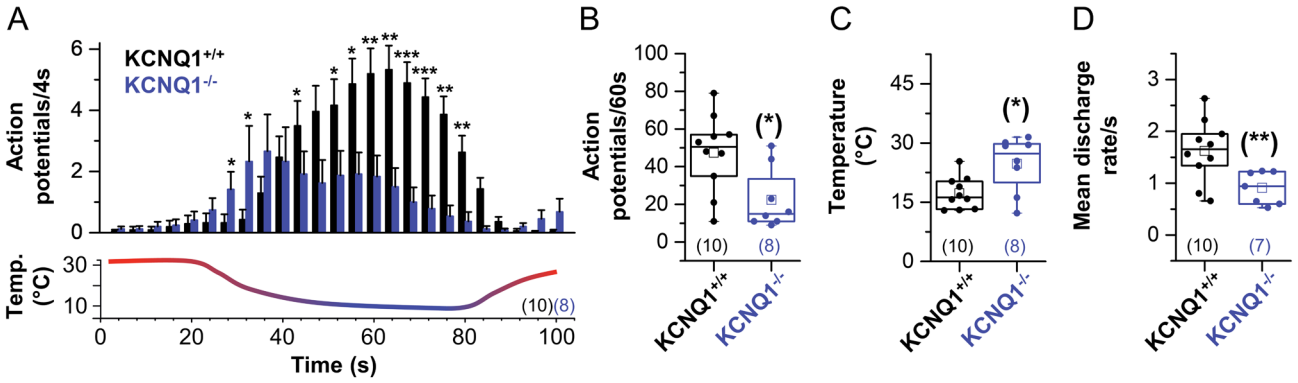

Fig. 5. Altered cold response in KCNQ1-deficient C-fibers. (*A*) Histogram of the average action potentials recorded as a cold response (in 4 s bins) of male *KCNQ1*$^{-/-}$ (blue) and matched wild-type littermates, *KCNQ1*$^{+/+}$ (black). The applied cold stimuli are plotted below the histogram. (*B–D*) Box plots illustrate the data distribution of (*B*) the response magnitude (in action potentials during the 60 s cold stimulus), (*C*) the activation threshold (in °C temperature), and (*D*) the mean discharge rate. The number of biological replicates (n) is indicated within the graphs. Squares: mean, line: median, box: 25 to 75%, and whiskers: 1.5 times the IQR. Data are presented as mean ± SEM in panel *A*. *P < 0.05, **P < 0.01, ***P < 0.001 by Mann–Whitney U-Test.

relevant for assigning menthol-mediated effects to KCNQ1. For instance, Rozza et al. described a gastroprotective role for menthol by an unknown mechanism of action (56). As acid secretion requires KCNQ1-mediated potassium recycling in parietal cells (57), the gastroprotective effect of menthol may result from the inhibition of KCNQ1.

Sex differences in thermal sensitivity are well documented, and in humans and mice, females prefer warmer conditions compared to males (19–21). We found a thermal preference of male *KCNQ1*$^{-/-}$ mice that was absent in female animals. Thus, *KCNQ1* is the first gene playing a role in sex-specific temperature sensation. KCNQ1 may be differentially expressed and regulated in the peripheral nervous system and may account for this sex-specific effect. Strikingly, there is already growing evidence for a sex-specific regulation of KCNQ1, albeit outside the nervous system. In humans, females have in some tissue significantly lower levels of KCNQ1 or KCNE1 mRNA transcripts (22, 23). Consistently, females have longer QT intervals in the cardiac surface ECG (58). Here, also nongenomic effects might contribute to the sexual differences, as testosterone directly activates the cardiac I_{Ks} channel complex formed by the KCNQ1/KCNE1 channel complex in males (24), while estradiol causes an inhibition of I_{Ks} in females (25). Strikingly, estradiol can modulate cold responses in female rats (59) and suppress menthol-induced increases in body temperature (60). If mice also have similar differences in sex-specific KCNQ1 expression and regulation as humans, female animals may already have other mechanisms for cold avoidance at baseline.

We found that the temperature dependence of native I_{Ks} in cardiomyocytes is best recapitulated in *Xenopus* oocytes, whereas the temperature regulation is almost completely lost in CHO cells (34). When we analyzed the temperature sensitivity of KCNQ1 in a mammalian cell line, transfected with KCNQ1, the temperature sensitivity of the channel was, similarly to that of I_{Ks}, almost completely lost (Q_{10} of about 2.2). This finding is in agreement with the aforementioned study by Seebohm et al., and suggests that transfected mammalian cell lines may not be well suited to predict the Q_{10} value of I_{Ks} in native cells (34). Another study found that the KCNQ1 channel alone is less temperature sensitive than in combination with the KCNE1 β-subunit (35). However, these experiments were performed in an unpaired manner by analyzing the activation kinetics of these channels at different temperatures and in CHO cells, in which both KCNQ1 and KCNQ1 plus KCNE1 are almost not temperature sensitive per se. Therefore, we considered it as the best approach to analyze the temperature sensitivity of KCNQ1 expressed alone in *Xenopus* oocytes, since in this cell system, the correlation between native I_{Ks} and I_{Ks} reconstituted by coexpression of KCNQ1 plus KCNE1 was the best (34). Q_{10} values may depend on the membrane potential, and we measured at very depolarized potentials. However, since endogenous L-type Ca^{2+} currents in *Xenopus* oocytes peak at about 0 mV and induce a potential contamination by calcium-activated chloride channels, we minimized the influence of other endogenous currents that could interfere with temperature-sensitivity measurements by recording at +40 mV. Nevertheless, the actual temperature sensitivity of KCNQ1 determined at +40 mV in the heterologous oocyte expression systems may differ from that in native DRG neurons.

One might expect an increase in basal action potential frequency in *KCNQ1*$^{-/-}$ mice due to the ability of the channels to contribute to the negative resting membrane potential in DRGs.

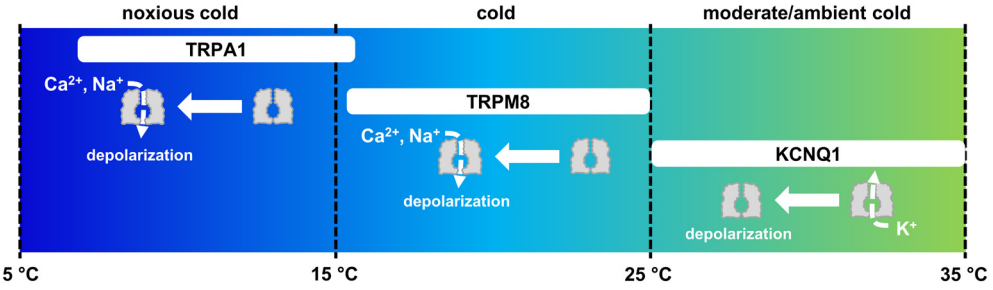

Fig. 6. Primary cold sensors at different temperature ranges. KCNQ1 potassium channels primarily sense moderate/ambient cold temperatures, while TRPM8 channels primarily detect cold and TRPA1 channels noxious cold temperatures. The cartoon illustrates that upon cooling TRP channels conduct increased cationic inward currents to depolarize membranes and transduce cold signals, while in KCNQ1 positive DRG neurons, the membrane depolarization to transduce cold signals is caused by reduced outward potassium currents.

Differences in the basal action potential frequency at 32 °C skin temperature have been observed in *TRAAK* single and *TRAAK* and *TREK-1* double knock-out animals using skin nerve recordings (12). Therefore, the absence of KCNQ1 may also lead to an increase in action potential frequency; however, we did not observe such effects in *TREK-1* single knock-out animals for example. Compensatory processes may be an explanation for differences in the basal action potential frequencies. Such compensations may be provided by other potassium channel subtypes and may be in place to prevent an over excitation and persistent "cold" signaling at warm ambient temperatures. We speculate that upregulation of another, not menthol-sensitive, potassium conductance may protect C-fibers from over excitation at rest, yet, the menthol-sensitive depolarizations by block of KCNQ1 channels and the respective cold-signals are strongly diminished.

Our study raises the question whether LQT1 patients suffer from an altered thermoreception and whether this might be also observed preferentially in male patients. In addition, a putative phenotype in thermosensation might be absent in heterozygous Roman-Ward syndrome and present only in recessive Jervell-Lange-Nielsen syndrome. However, clinical studies addressing these questions would require a large cohort of LQT1 patients of both sexes and patients with another type of LQT syndrome as control. A comparison with LQT2 would make sense since the patients have the same underlying disease and a similar medication, but the loss-of-function is in the *KCNH2* gene instead of the *KCNQ1* gene.

The physiological sensation of cold temperatures is likely to involve not only TRPM8 but an extensive array of other ion channels that contribute to and modulate the threshold and intensity of perception. Strikingly, many cold-sensitive peripheral neurons do not even express TRPM8 channels (3) and there is a residual menthol and cold sensitivity in *TRPM8*-deficient mice (4–6). In addition, even though that different types of ion channels were discussed to modulate cold signaling, the role of these channels in cold sensation has remained unclear, primarily due to a lack of strong effects on temperature sensation in an appropriate in vivo assay. Based on the finding of a functional expression in C-fibers, the strong temperature- and menthol-sensitivity, together with the strong in vivo effects on cold avoidance, we propose an extracardiac function for KCNQ1 channels, namely the perception of moderate/ambient cold temperatures in a sex-dependent manner. Thus, KCNQ1, together with TRPM8, which is active at cooler temperatures, might work in concert to cover the whole range of nonnoxious cold-sensation in a sex-dependent manner.

Materials and Methods

Animals. Eleven *KCNQ1*$^{-/-}$ and 14 *KCNQ1*$^{+/+}$ male mice weighing between 18 and 32 g were used for behavioral temperature preference testing, C-fiber recording, and for immunohistochemistry. An additional 5 male and 10 female *KCNQ1*$^{-/-}$ and 13 female *KCNQ1*$^{+/+}$ mice were used for behavioral temperature preference testing. One male *TRPM8*$^{EGFPf/EGFPf}$ mouse was used for immunohistochemistry. Transgenic animals were conventionally genotyped using commercially available primers as described in the literature (16). *TRPM8*$^{EGFPf/EGFPf}$ mice were kindly provided by Ardem Patapoutian (The Scripps Research Institute, San Diego, CA) (61). Mice were maintained at a constant room temperature (22 °C) and humidity between 40 and 60% under a 12-h light/dark cycle and food and water were provided ad libitum. Mice were culled by 100% CO_2 and cervical dislocation for C-fiber recording and immunohistochemistry. The protocol for in vivo experiments in animals was reviewed by the local animal ethics committee (University of Erlangen) and approved by the local district government of Middle Franconia (55.2-2532.1-29/10). In addition, animal experiments with mice were approved by the local authorities at the University of Tuebingen (Regierungspräsidium Tuebingen, PY114) and animal experiments with *Xenopus* toads at the University of Marburg (Regierungspräsidium Giessen, MR 20/28 Nr. A 23/2017).

Two Electrode Voltage-Clamp Recordings in *Xenopus laevis* Oocytes. Oocytes were isolated from anesthetized *Xenopus laevis* frogs (Nasco, Wisconsin) and incubated in OR2 solution containing in mM: NaCl 82.5, KCl 2, $MgCl_2$ 1, HEPES 5 (pH 7.5) supplemented with 2 mg/mL collagenase II (Sigma, Hamburg, Germany) to remove residual connective tissue. Oocytes were then stored at 18 °C in ND96 solution supplemented with 50 mg/L gentamicin, 274 mg/L sodium pyruvate, and 88 mg/L theophylline. Channels and mutants were subcloned into pSP64, pXOOM, pSGEM, pcDNA, or pTLN vectors. Mutations in human KCNQ1 cDNA were introduced using the QuikChange Site-Directed Mutagenesis Kit (Stratagene, La Jolla, CA) according to the manufacturer's instructions, or clones were obtained from Michael C. Sanguinetti, University of Utah, USA. cDNA was linearized with NheI, EcoRI, and PvuI, respectively, and cRNA was synthesized using the mMESSAGE mMACHINE-Kit (Ambion, Carlsbad, CA). All genotypes used were human except Kv1.4 (rat). Quantity and quality of cRNAs were assessed by gel electrophoresis and spectroscopy (NanoDrop 2000c, Thermo Fisher Scientific, Waltham, MS), respectively. Each oocyte was injected with 50 nL cRNA. Two electrode voltage-clamp recordings were performed at room temperature (20 to 22 °C), or the temperature was controlled by cooling or heating the bath solution with a TC-10 temperature control system. Recordings were made using a TurboTEC 10CD (npi, Tamm, Germany) amplifier and a Digidata 1200 Series (Molecular Devices, Sunnyvale, CA) A/D converter. Micropipettes were made from GB 150TF-8P borosilicate glass capillaries (Science Products, Millville, NJ) and pulled with a DMZ-Universal Puller (Zeitz, Martinsried, Germany). The recording pipettes had a resistance of 0.5 to 1.5 MΩ when filled with 3 M KCl solution. The recording solution ND96 contained in mM: NaCl 96, KCl 2, $CaCl_2$ 1.8, $MgCl_2$ 1, HEPES 5 (pH 7.5). Drugs were diluted in DMSO, and the final concentration of DMSO in the applied drugs was less than 0.1%. All drugs were applied through a laminar flow driven by gravity. The drug block was analyzed with a voltage step from a holding potential of −80 mV followed by a 1 s pulse to +40 mV. The sweep time interval was 10 s. For menthol block of the KCNQ4 channel and temperature sensitivity of the KCNQ1 channel, the depolarizing pulse was 3 s. TRAAK and TREK-1 channels were recorded with a voltage ramp from a holding potential of −80 mV first to -120 mV in 0.1 s and then to +40 mV in 3.5 s. The sweep time interval for this protocol was 10 s. For temperature sensitivity analysis, the time course of current activation was recorded continuously while the bath was heated from 14 to 37 °C at 1 °C/min. The relative current amplitudes was calculated at the end of the depolarizing pulse. These peak currents were used to determine temperature sensitivity with Q_{10} values for 15 to 25 °C and 25 to 35 °C according to Cui et al. (62). Q_{10} values were calculated for the fixed regions to emphasize the change in temperature sensitivity within the physiological range.

Cell Culture. HeLa cells were grown to ∼50% confluence on 35 mm dishes (NUNC). Cells were transfected with 1 μg KCNQ1 pCDNA3.1(-) and 0.5 μg pEGFP cDNA using Jetprime (PEQLAB). Recordings were done 24 to 30 h after transfection.

Patch-Clamp Electrophysiology. All patch-clamp recordings were performed at room temperature (20 to 22 °C). Voltage clamp data were recorded using an Axopatch 200B amplifier and a Digidata 1440A A/D converter (Molecular Devices, Sunnyvale, CA) or HEKA EPC 10 system (Multi Channel Systems, Stuttgart, Germany). Pipettes were made of GB 150TF-8P borosilicate glass capillaries (Science Products, Millville, NJ), pulled with a DMZ-Universal Puller (Zeitz, Martinsried, Germany) and had a resistance of 3 to 5 MΩ. The pipette solution contained in mM: KCl 60, K-glutamate 65, $MgCl_2$ 2, EGTA 5, K_2ATP 3, Na_2GTP 0.2, and HEPES 5 for HeLa whole-cell patch-clamp recordings. The pH was adjusted to 7.2 with KOH. (-)-menthol or WS-12 was dissolved in a bath solution containing in mM: NaCl 135, KCl 5, $MgCl_2$ 1, $CaCl_2$ 1, NaH_2PO_4 0.33, Glucose 10, Na-Pyruvate 2, and HEPES 10 for HeLa whole-cell patch-clamp recordings. pH was adjusted to 7.4 with NaOH.

Molecular Modeling. A consensus open KCNQ1 homology model was generated similar to that described previously (63). Briefly, a consensus KCNQ1 homology model was generated based on the results of a pdb database search using PSI-BLAST (64), including amino acids 89–358. Identified templates 2a79

and 2r9r were ranked based on alignment scores and structural quality estimates according to WHAT_CHECK (65) obtained from the PDBFinder2 database (66). The top scoring templates 2a79 and 2r9r were aligned to the KCNQ1 sequence and iteratively optimized using evolutionary information contained in related sequences (SwissProt and TrEMBL) (67). Structure-based alignment correction, based in part on SSALN scoring matrices, was applied (68). Optimal loop anchor points were determined to collect possible loop conformations, and insertions, deletions, and dead-end elimination were used to find an initial rotamer solution using a simple repulsive energy function, which was then loop optimized using YASARA algorithms (69). Side-chain rotamer fine-tuning was performed, taking into account electrostatic, knowledge-based packing, and solvation effects. Unrestrained high-resolution refinement with explicit solvent molecules was performed using the AMBER03 force field, and the result was validated using YASARA. The final hybrid model was constructed, and bad regions in the top-scoring model were iteratively replaced with corresponding fragments from the other models. The resulting consensus homology model comprises amino acids 89–358 of KCNQ1. Five different independent menthol models were generated. The following specific parameters were selected for KCNQ1 modeling: slow modeling speed, 6 PSI-BLAST iterations in template search, $E_{Value\ Max}$: 0.5, 50 conformations tried per loop (LoopSamples), 10 residues added to the termini (TermExtension). Energy-optimized menthol conformers were manually docked to the KCNQ1 homology model in close proximity to the identified residues within the central cavity, and the resulting KCNQ1–menthol complexes were energy-minimized. The lowest energy complex was selected for a final molecular dynamics simulation. The KCNQ1–menthol model complex was placed in a simulation box and inserted into a virtual, mixed membrane consisting of equal amounts of phosphatidylethanolamine (PEA), phosphatidylcholine (PCH), and phosphatidylserine (PSE; PEA/PCH/PSE–33%/33%/33%). The membrane height was 43 Å (density ~0.861 g/L), and the height of the hydrophobic membrane core was 28 Å. The KCNQ1–menthol model was shrunk to 50% of its size, and lipids that bumped into the shrunken protein were deleted. The size of the KCNQ1–menthol complex was gradually expanded to reach regular size and completely fill the membrane pore. Each expansion step was followed by energy minimization. The simulation box was filled with water, and 0.9% NaCl was added to the system. Then, 1.575 ns MD simulations were performed on the KCNQ1–menthol complex. The following simulation settings were used for the molecular dynamics simulation: force field: AMBER-03, temperature: 298° K, pressure: 1 bar, pH 7.0, Coulomb electrostatic cutoff: 7.86, 0.9% NaCl, solvent density: 0.997, 1 fs time steps, periodic boundaries, all atoms mobile. The average structure was determined from the simulation and used to calculate RMSFs for each model. RMSD and energies were also calculated. The membrane was artificially stabilized during an initial equilibration period of 25 ps so that it could repack and cover the solute, while solvent water molecules were kept outside the membrane core for the first 250 ps of the simulation.

RT-PCR of Human Skin. For the KCNQ1–5 expression profile, RT-PCR was performed using illustra, PuReTaq, Ready-To-Go PCR Beads (GE Healthcare). The kits were used according to the manufacturer's specifications. PCR products were analyzed by agarose gel electrophoresis and verified by complete DNA sequencing of the PCR fragments. KCNQ1–5 specific primers used for PCR of human skin cDNA (human skin cDNA, ZYAGEN Catalog #: HD–101) were designed to span an intron. Primer sequences: KCNQ1 F, 5′-AGTTCAAGCTGGACAAAGAC AATGG–3′; KCNQ1 R, 5′-TGTGAGATGTGGGTGATGGGTG-3′; KCNQ2 F, 5′–ACCG TTCTGTGTGATTGACATCATG–3′; KCNQ2 R, 5′–AAGTACACCAGGAACGAGGCC–3′; KCNQ3 F, 5′–AAGGCAATGTTCTGGCCACCTC–3′, KCNQ3 R, 5′–TCTCCTCTCCTTGTGCA TCCAC–3′; KCNQ4 F, 5′–AGCATCTGGCACCTCCAACAATG–3′; KCNQ4 R, 5′–TGATGGAGC GG ATGACTGTCTTC–3′; KCNQ5 F, 5′–ACAGCCCTTGGCACTGATGATG–3′; KCNQ5 R, 5′–TTCTACACAACATGTCCAGATGACC–3′. For the experiments comparing the KCNQ1 expression to that of TRPM8, human skin total RNA (amsbio, Catalog #: R1234218–50) was reverse transcribed using SuperScript™ II Reverse Transcriptase (ThermoFisher, Invitrogen) and Oligo(dT)12–18 Primer (ThermoFisher, Invitrogen). RT-PCR was performed using AmpliTaq Gold™ DNA-Polymerase (ThermoFisher, Applied Biosystems) and intron-spanning primers: hTRPM8 F, 5′–TTGTCTGGAAACTGGTTGCGAA–3′, hTRPM8 R, 5′–GGTGCCGAGTAATAGGAGACAC–3′, hKCNQ1 F, 5′–TGGAGAGAAG ATGCTCACAG–3′, hKCNQ1 R, 5′–TGTTGGGCTCTTCCTTACAG–3′. Pixel-densitometry analysis was performed using the ImageJ software (NIH).

Primary Culture of Dorsal Root Ganglia. DRG neurons were isolated from all levels of the spinal cord of adult male *KCNQ1*$^{-/-}$ and *TRPM8*$^{EGFPf/EGFPf}$ mice. Neurons were harvested in 0.6 mg/mL collagenase (type XI, Sigma Aldrich, Munich, Germany) and 3 mg/mL protease (Sigma) for 40 min at 37 °C in DMEM. Cells were washed three times, triturated, and plated on poly-D-lysine (0.1 mg/mL) borosilicate glass coverslips in serum-free TNB-100 basal medium (Biochrom AG, Berlin, Germany), supplemented with penicillin, streptomycin, and 100 ng/mL nerve growth factor-7S (Alomone Labs, Jerusalem, Israel).

Western Blot Analysis. HeLa cells were washed in PBS and harvested 48 h after transfection using a buffer containing 150 mM NaCl, 50 mM TRIS (pH 7.5), 1% (v/v) Triton X-100 supplemented with protease inhibitor cocktail. Cells were incubated 30 min on ice and subsequently cleared by centrifugation (13,000 rpm at 4 °C for 15 min). Subsequently, proteins were size-separated on 12% SDS polyacrylamid gels and transferred onto nitrocellulose membrane. The membrane was blocked in TBST (50 mM Tris-HCl, pH 7.5, 150 mM NaCl, 0.1% Tween-20) containing 3% (w/v) BSA for 2 h at room temperature and stained with KCNQ1 antibodies (Santa Cruz Biotechnology, sc-20816, 1:1,000) over night at 4 °C. After three washing steps with TBST, the blots were incubated for 1 h at room temperature with peroxidase-coupled goat anti-rabbit antibody (31460, ThermoFisher Scientific, 1:8,000). After washing with TBST, signals were detected applying SuperSignal™ West Dura Extended Duration Substrate (ThermoFisher Scientific).

Immunohistochemistry of Primary Cultures of Dorsal root ganglia. After incubation for 4 h, cells were fixed with 4% paraformaldehyde (Sigma-Aldrich) in phosphate-buffered saline (PBS) (Gibco) for 30 min. The cells were washed three times with PBS at room temperature. After blocking and permeabilization with 1% BSA (Carl Roth GmbH) + 5% normal goat serum (Vector Laboratories Inc.) + 0.5% Triton X-100 (Sigma-Aldrich) for 4 h at 4 °C, DRG cells were immunostained with anti-KCNQ1 primary antibody (H-130, sc-20816; Santa Cruz Biotechnology, Heidelberg, Germany) (1:500) in PBS containing 1% BSA and 0.5% Triton X-100 overnight at 4 °C. Primary antibody dilutions of 1:1,000 and 1:5,000 were also tested but resulted in a low signal. After three washes with PBS, the culture was incubated with goat anti-rabbit Cy3 secondary antibody (Abcam) for 4 h and washed three more times with PBS. The coverslips were then mounted on glass slides using Roti-Mount FluorCare DAPI mounting medium (Carl Roth).

Thermal Preference Assay. Behavioral data were collected in a custom-designed circular gradient assay assembled in the small configuration as previously described (43). Briefly, the apparatus consists of an annular 1.5 cm thick aluminum disk, and the dimensions of the inner and outer ring diameters were 28 cm and 40 cm, respectively. The inner walls were made of transparent Plexiglas and the outer walls of aluminum (to mask positional cues), both 12 cm high with circumferences of 88 cm and 126 cm, respectively. The inner circular surface was 10 cm wide, where a temperature gradient was equilibrated and the mouse was placed to move freely. The surface of the ring was made of anodized aluminum (colored orange) with low-light reflection to provide sufficient contrast for mouse detection but also to allow surface temperature control with an infrared camera. During the measurements, the relevant areas were uniformly illuminated, and the mouse behavior was videotaped with a standard CCD camera. The thermal gradient was constantly equilibrated across the aluminum disk using two feedback-controlled peltier-based plates (TE Technology, Traverse City, MI) in combination with a custom-made temperature controller (Labortechnik Franken, Röthenbach, Germany) as described previously (43). The stability of the surface temperature gradient was monitored with an infrared camera (T400 series, FLIR® Systems GmbH, Frankfurt, Germany) prior to each measurement. Deviations of less than ±1.7 °C were tolerated but readjusted. The apparatus was closed with a transparent cover with radial lines to divide the small ring into 15 equal-sized zones and one larger zone. Each individual zone covered an area of 40 cm^2, while the one larger zone covered 80 cm^2 and marked the coldest area. This was necessary for unambiguous offline analysis of the videotaped behavior using custom-designed software (43). The symmetrical arrangement resulted in two semicircles of equal temperature on opposite sides. Consequently, values for each thermal zone were provided in duplicate, and two equal-temperature zones were summed to obtain the preference temperature. Data were subjected to a three-point averaging procedure and pooled for the semicircles to obtain time courses of thermal selection. The cumulative response function was calculated from the individual zone occupancies.

C-Fiber Recordings. We used the isolated skin-saphenous nerve preparation and single-fiber recording technique together with the DAPSYS software (Brian Turnquist, turnquist@bethel.edu, https://www.dapsys.net/) and a DAP5200a/626 board (Microstar Laboratories, Bellevue, WA) as described previously (70). We recorded from preparations of male C57BL/6J-based *KCNQ1*$^{-/-}$ mice and used littermates born from breeding cages of parental heterozygous mice. Skin was maintained under laminar superfusion of carbogen-gassed synthetic interstitial fluid (SIF). SIF, pH 7.4, contained (in mM) 108 NaCl, 3.5 KCl, 3.5 $MgSO_4$, 26 $NaHCO_3$, 11.7 NaH_2PO_4, 1.5 $CaCl_2$, 9.6 sodium gluconate, 5.6 glucose, and 7.6 sucrose. Receptive fields of mechanosensitive C-fibers were searched by stimulation with a blunt glass rod and isolated with a Teflon ring. Thermal stimuli were applied as a 20 s ramp from 30 to 50 °C or as a 60 s negative exponential decay from 30 to 5 °C. The criterion for assigning cold responsiveness to a fiber was a discharge of at least five APs during 60 s of cold stimulation. We used a previously described custom-made countercurrent temperature exchange application system to apply the thermal stimuli and superfused the receptive fields at a rate of 10 mL/min (70). The temperature was measured with a 0.25 mm thin thermocouple (Omega, Deckenpfronn, Germany) placed directly above the receptive field at the outlet opening. Superfusion fluid was applied directly to the surface of the receptive field to avoid thermal gradients from the center of the ring radially outward. Cold sensitivity was assigned to all cold responses with a discharge of >5 spikes and a static component during the 60 s cold stimulation. The activation threshold was the temperature at which the first spike in a series of action potentials was discharged, usually the first spike of the static part of the response. Data points were subjected to a three-point averaging procedure.

Confocal Microscopy and Data Analysis. Confocal microscopy of DRG inserts was performed using a Zeiss Spinning Disc Axio Observer Z1. After thresholding the images, cells were analyzed using the analyze particles function of Image J. Coexpression was tested using a custom-written script in ImageJ.

Data Analysis and Statistics. All electrophysiological data were acquired with Clampex (Molecular Devices, Sunnyvale, CA) and analyzed with Clampfit 10 (Molecular Devices, Sunnyvale, CA), Origin (OriginLab Corp, Northampton, MS), and Excel (Microsoft Corp, Seattle, WA). The respective graphs indicate the number of biological replicates (n) as small insets. All values are expressed as mean ± SEM unless otherwise noted. Asterisks indicate significance: $*P < 0.05$; $**P < 0.01$; $***P < 0.001$. Significance was assessed by a two-tailed Student's *t* test, unless otherwise indicated. ANOVA for multiple comparisons was used for the temperature sensitivity assay. ANOVA revealed significant effects of all factors, genotype ($P = 0.009$), sex ($P = 0.029$), and time ($P < 0.0001$), but no interactions.

Data, Materials, and Software Availability. All information and methods to reproduce our data are provided within the manuscript. No codes are reported in this study. The following KCNQ1 clones used in the current study were deposited in Addgene: KCNQ1 in pSGEM (Addgene ID #219952) (71) and in pCDNA3.1 (Addgene ID #219953) (72). All other data are included in the manuscript and/or supporting information. Some study data available (Any request, i.e. for materials like clones, will be answered by us and all material will be provided).

ACKNOWLEDGMENTS. A.K.K. was supported by the Grant 67-0015 of the Von-Behring-Röntgen-Stiftung. N.D. is supported by the Grant DE1482-9/1 of the Deutsche Forschungsgemeinschaft. S.S. is supported by the Studienstiftung des Deutschen Volkes e.V. C.S. is supported by Else-Kröner Fresenius Foundation Clinician-Scientist professorship. We thank Simone Preis, Oxana Nowak, Vanessa Huhn, Andrea Schubert, and Jana Schramm for technical assistance.

Author affiliations: [a]Institute for Physiology and Pathophysiology, Department of Vegetative Physiology and Center for Mind, Brain and Behavior, Philipps-University Marburg, 35032 Marburg, Germany; [b]Department of Anesthesiology, University of Erlangen-Nürnberg, 91054 Erlangen, Germany; [c]Institute for Anatomy and Cell Biology, Department of Medicinal Cellbiology and Center for Mind, Brain and Behavior, Philipps-University Marburg, 35032 Marburg, Germany; [d]Department of Cytology, Institute of Anatomy, Ruhr-University Bochum, 44801 Bochum, Germany; [e]Faculty of Chemistry and Biochemistry, Department of Receptor Biochemistry, Ruhr-University Bochum, 44780 Bochum, Germany; [f]Institute for Physiology I, Department of Physiology I, Eberhard Karls University Tübingen, 72074 Tübingen, Germany; [g]Department of Cardiology, University Hospital Heidelberg, 69120 Heidelberg, Germany; [h]Department for Genetics of Heart Diseases (IfG), University Hospital Münster, 48149 Münster, Germany; and [i]Institute for Physiology and Pathophysiology, Department of Physiology, Johannes Kepler University Linz, 4040 Linz, Austria

1. H. Hensel, Y. Zotterman, The effect of menthol on the thermoreceptors. *Acta Physiol. Scand.* **24**, 27–34 (1951).
2. D. D. McKemy, W. M. Neuhausser, D. Julius, Identification of a cold receptor reveals a general role for TRP channels in thermosensation. *Nature* **416**, 52–58 (2002).
3. C. Munns, M. AlQatari, M. Koltzenburg, Many cold sensitive peripheral neurons of the mouse do not express TRPM8 or TRPA1. *Cell Calcium* **41**, 331–342 (2007).
4. R. W. Colburn *et al.*, Attenuated cold sensitivity in TRPM8 null mice. *Neuron* **54**, 379–386 (2007).
5. A. Dhaka *et al.*, TRPM8 is required for cold sensation in mice. *Neuron* **54**, 371–378 (2007).
6. D. M. Bautista *et al.*, The menthol receptor TRPM8 is the principal detector of environmental cold. *Nature* **448**, 204–208 (2007).
7. Y. Karashima *et al.*, Bimodal action of menthol on the transient receptor potential channel TRPA1. *J. Neurosci.* **27**, 9874–9884 (2007).
8. Y. Karashima *et al.*, TRPA1 acts as a cold sensor in vitro and in vivo. *Proc. Natl. Acad. Sci. U.S.A.* **106**, 1273–1278 (2009).
9. Z. Winter, P. Gruschwitz, S. Eger, F. Touska, K. Zimmermann, Cold temperature encoding by cutaneous TRPA1 and TRPM8-carrying fibers in the mouse. *Front. Mol. Neurosci.* **10**, 209 (2017).
10. K. Zimmermann *et al.*, Transient receptor potential cation channel, subfamily C, member 5 (TRPC5) is a cold-transducer in the peripheral nervous system. *Proc. Natl. Acad. Sci. U.S.A.* **108**, 18114–18119 (2011).
11. L. Bernal *et al.*, Odontoblast TRPC5 channels signal cold pain in teeth. *Sci. Adv.* **7**, eabf5567 (2021).
12. J. Noël *et al.*, The mechano-activated K^+ channels TRAAK and TREK-1 control both warm and cold perception. *EMBO J.* **28**, 1308–1318 (2009).
13. V. Pereira *et al.*, Role of the TREK2 potassium channel in cold and warm thermosensation and in pain perception. *Pain* **155**, 2534–2544 (2014).
14. A. Castellanos *et al.*, TRESK background K. *J. Physiol.* **598**, 1017–1038 (2020).
15. C. Morenilla-Palao *et al.*, Ion channel profile of TRPM8 cold receptors reveals a role of TASK-3 potassium channels in thermosensation. *Cell Rep.* **8**, 1571–1582 (2014).
16. I. Vetter *et al.*, Amplified cold transduction in native nociceptors by M-channel inhibition. *J. Neurosci.* **33**, 16627–16641 (2013).
17. F. Viana, E. de la Peña, C. Belmonte, Specificity of cold thermotransduction is determined by differential ionic channel expression. *Nat. Neurosci.* **5**, 254–260 (2002).
18. A. Alloui *et al.*, TREK-1, a K^+ channel involved in polymodal pain perception. *EMBO* **J.25**, 2368–2376 (2006).
19. Q. Zhao, J. Lyu, H. Du, Z. Lian, Z. Zhao, Gender differences in thermal sensation and skin temperature sensitivity under local cooling. *J. Therm. Biol.* **111**, 103401 (2023).
20. K. Kaikaew *et al.*, Sex difference in cold perception and shivering onset upon gradual cold exposure. *J. Therm. Biol.* **77**, 137–144 (2018).
21. K. Kaikaew, J. Steenbergen, A. P. N. Themmen, J. A. Visser, A. Grefhorst, Sex difference in thermal preference of adult mice does not depend on presence of the gonads. *Biol. Sex. Differ.* **8**, 24 (2017).
22. E. Moric-Janiszewska *et al.*, Age-and sex-dependent mRNA expression of KCNQ1 and HERG in patients with long QT syndrome type 1 and 2. *Arch. Med. Sci.* **7**, 941–947 (2011).
23. N. Gaborit *et al.*, Gender-related differences in ion-channel and transporter subunit expression in non-diseased human hearts. *J. Mol. Cell. Cardiol.* **49**, 639–646 (2010).
24. C.-X. Bai, J. Kurokawa, M. Tamagawa, H. Nakaya, T. Furukawa, Nontranscriptional regulation of cardiac repolarization currents by testosterone. *Circulation* **112**, 1701–1710 (2005).
25. C. Möller, R. Netzer, Effects of estradiol on cardiac ion channel currents. *Eur. J. Pharmacol.* **532**, 44–49 (2006).
26. M. C. Sanguinetti *et al.*, Coassembly of K_VLQT1 and minK (IsK) proteins to form cardiac I_{Ks} potassium channel. *Nature* **384**, 80–83 (1996).
27. J. Barhanin *et al.*, K_VLQT1 and IsK (minK) proteins associate to form the I_{Ks} cardiac potassium current. *Nature* **384**, 78–80 (1996).
28. Q. Wang *et al.*, Positional cloning of a novel potassium channel gene: *K_VLQT1* mutations cause cardiac arrhythmias. *Nat. Genet.* **12**, 17–23 (1996).
29. M. A. Sherkheli *et al.*, Characterization of selective TRPM8 ligands and their structure activity response (S.A.R) relationship. *J. Pharm. Pharm. Sci.* **13**, 242–253 (2010).
30. H. S. Wang *et al.*, KCNQ2 and KCNQ3 potassium channel subunits: Molecular correlates of the M-channel. *Science* **282**, 1890–1893 (1998).
31. C. Lerche *et al.*, Chromanol 293B binding in KCNQ1 (Kv7.1) channels involves electrostatic interactions with a potassium ion in the selectivity filter. *Mol. Pharmacol.* **71**, 1503–1511 (2007).
32. N. Decher *et al.*, Molecular basis for Kv1.5 channel block. *J. Biol. Chem.* **279**, 394–400 (2004).
33. A. E. Busch, F. Lang, Effects of $[Ca^{2+}]_i$ and temperature on minK channels expressed in *Xenopus* oocytes *FEBS Lett.* **334**, 221–224 (1993).
34. G. Seebohm, C. Lerche, A. E. Busch, A. Bachmann, Dependence of I_{Ks} biophysical properties on the expression system. *Pflügers Arch.* **442**, 891–895 (2001).
35. B. Unsöld *et al.*, KCNE1 reverses the response of the human K^+ channel KCNQ1 to cytosolic pH changes and alters its pharmacology and sensitivity to temperature. *Pflügers Arch.* **441**, 368–378 (2000).
36. S. Brauchi, P. Orio, R. Latorre, Clues to understanding cold sensation: Thermodynamics and electrophysiological analysis of the cold receptor TRPM8. *Proc. Natl. Acad. Sci. U.S.A.* **101**, 15494–15499 (2004).
37. M. Elias, G. Wieczorek, S. Rosenne, D. S. Tawfik, The universality of enzymatic rate-temperature dependency. *Trends Biochem. Sci.* **39**, 1–7 (2014).
38. A. M. Goldman *et al.*, Arrhythmia in heart and brain: KCNQ1 mutations link epilepsy and sudden unexplained death. *Sci. Trans. Med.* **1**, 2ra6 (2009).
39. A. Jervell, F. Lange-Nielsen, Congenital deaf-mutism, functional heart disease with prolongation of the Q-T interval and sudden death. *Am. Heart J.* **54**, 59–68 (1957).
40. M. Uhlén *et al.*, Tissue-based map of the human proteome. *Science* **347**, 1260419 (2015).

41. D. Usoskin *et al.*, Unbiased classification of sensory neuron types by large-scale single-cell RNA sequencing. *Nat. Neurosci.* **18**, 145–153 (2015).
42. N. Sharma *et al.*, The emergence of transcriptional identity in somatosensory neurons. *Nature* **577**, 392–398 (2020).
43. F. Touska *et al.*, Comprehensive thermal preference phenotyping in mice using a novel automated circular gradient assay. *Temperature (Austin)* **3**, 77–91 (2016).
44. M. Wilhelm *et al.*, Mass-spectrometry-based draft of the human proteome. 509, 7502 (2014).
45. D. M. Ribeiro, C. Ziyani, O. Delaneau, Shared regulation and functional relevance of local gene co-expression revealed by single cell analysis. *Commun. Biol.* **5**, 876 (2022).
46. A. L. Bauernfeind, C. C. Babbitt, The predictive nature of transcript expression levels on protein expression in adult human brain. *BMC Genomics* **18**, 322 (2017).
47. G. M. Passmore *et al.*, KCNQ/M currents in sensory neurons: Significance for pain therapy. *J. Neurosci.* **23**, 7227–7236 (2003).
48. P. Rivas-Ramírez, A. Reboreda, L. Rueda-Ruzafa, S. Herrera-Pérez, J. A. Lamas, Contribution of KCNQ and TREK channels to the resting membrane potential in sympathetic neurons at physiological temperature. *Int. J. Mol. Sci.* **21**, 5796 (2020).
49. J. Robbins, KCNQ potassium channels: Physiology, pathophysiology, and pharmacology. *Pharmacol. Ther.* **90**, 1–19 (2001).
50. L. V. Kristensen, K. Sandager-Nielsen, H. H. Hansen, Kv7 (KCNQ) channel openers induce hypothermia in the mouse. *Neurosci. Lett.* **488**, 178–182 (2011).
51. T. N. Griffith, T. A. Docter, E. A. Lumpkin, Tetrodotoxin-sensitive sodium channels mediate action potential firing and excitability in menthol-sensitive Vglut3-lineage sensory neurons. *J. Neurosci.* **39**, 7086–7101 (2019).
52. S. C. Liu *et al.*, The identification of the TRPM8 channel on primary culture of human nasal epithelial cells and its response to cooling. *Medicine (Baltimore)* **96**, e7640 (2017).
53. T. V. Kozyreva, G. M. Khramova, I. P. Voronova, A. A. Evtushenko, The influence of cooling and TRPM8 ion channel activation on the level of pro-inflammatory cytokines in normotensive and hypertensive rats. *J. Therm. Biol.* **61**, 119–124 (2016).
54. R. V. Olsen, H. H. Andersen, H. G. Møller, P. W. Eskelund, L. Arendt-Nielsen, Somatosensory and vasomotor manifestations of individual and combined stimulation of TRPM8 and TRPA1 using topical L-menthol and *trans*-cinnamaldehyde in healthy volunteers. *Eur. J. Pain* **18**, 1333–1342 (2014).
55. A. Teliban, F. Bartsch, M. Struck, R. Baron, W. Jänig, Responses of intact and injured sural nerve fibers to cooling and menthol. *J. Neurophysiol.* **111**, 2071–2083 (2014).
56. A. L. Rozza, C. A. Hiruma-Lima, R. K. Takahira, C. R. Padovani, C. H. Pellizzon, Effect of menthol in experimentally induced ulcers: Pathways of gastroprotection. *Chem. Biol. Interact.* **206**, 272–278 (2013).
57. P. Song *et al.*, KCNQ1 is the luminal K^+ recycling channel during stimulation of gastric acid secretion. *J. Physiol.* **587**, 3955–3965 (2009).
58. M. Merri, J. Benhorin, M. Alberti, E. Locati, A. J. Moss, Electrocardiographic quantitation of ventricular repolarization. *Circulation* **80**, 1301–1308 (1989).
59. Y. Uchida *et al.*, Estrogen modulates central and peripheral responses to cold in female rats. *J. Physiol. Sci.* **60**, 151–160 (2010).
60. Y. Uchida, K. Atsumi, S. Hirano, N. Koyanagi, Estradiol administration suppresses body temperature elevation induced by application of menthol to ovariectomized rats. *J. Therm. Biol.* **78**, 281–289 (2018).
61. A. Dhaka, T. J. Earley, J. Watson, A. Patapoutian, Visualizing cold spots: TRPM8-expressing sensory neurons and their projections. *J. Neurosci.* **28**, 566–575 (2008).
62. Y. Cui *et al.*, Selective disruption of high sensitivity heat activation but not capsaicin activation of TRPV1 channels by pore turret mutations. *J. Gen. Physiol.* **139**, 273–283 (2012).
63. N. Strutz-Seebohm *et al.*, Structural basis of slow activation gating in the cardiac I_{Ks} channel complex. *Cell Physiol. Biochem.* **27**, 443–452 (2011).
64. S. F. Altschul *et al.*, Gapped BLAST and PSI-BLAST: A new generation of protein database search programs. *Nucleic Acids Res.* **25**, 3389–3402 (1997).
65. R. W. Hooft, G. Vriend, C. Sander, E. E. Abola, Errors in protein structures. *Nature* **381**, 272 (1996).
66. R. W. Hooft, C. Sander, M. Scharf, G. Vriend, The PDBFINDER database: A summary of PDB, DSSP and HSSP information with added value. *Comput. Appl. Biosci.* **12**, 525–529 (1996).
67. R. D. King, M. J. Sternberg, Identification and application of the concepts important for accurate and reliable protein secondary structure prediction. *Protein Sci.* **5**, 2298–2310 (1996).
68. J. Qiu, R. Elber, SSALN: An alignment algorithm using structure-dependent substitution matrices and gap penalties learned from structurally aligned protein pairs. *Proteins* **62**, 881–891 (2006).
69. A. A. Canutescu, R. L. Dunbrack, Cyclic coordinate descent: A robotics algorithm for protein loop closure. *Protein Sci.* **12**, 963–972 (2003).
70. K. Zimmermann *et al.*, Phenotyping sensory nerve endings in vitro in the mouse. *Nat. Protocols* **4**, 174–196 (2009).
71. N. Decher, pSGEM hKCNQ1. AddGene. https://www.addgene.org/219952/. Deposited 15 April 2024.
72. N. Decher, pcDNA3.1(-) hKCNQ1. AddGene. https://www.addgene.org/219953/. Deposited 15 April 2024.